



# Succinylated Wheat Germ Agglutinin Colocalizes with the *Toxoplasma gondii* Cyst Wall Glycoprotein CST1

Rebekah B. Guevara,<sup>a</sup> Barbara A. Fox,<sup>a</sup> David J. Bzik<sup>a</sup>

<sup>a</sup>Department of Microbiology and Immunology, The Geisel School of Medicine at Dartmouth, Lebanon, New Hampshire, USA

**ABSTRACT** The glycosylated mucin domain of the *Toxoplasma gondii* cyst wall glycoprotein CST1 is heavily stained by *Dolichos biflorus* agglutinin, a lectin that binds to *N*-acetylgalactosamine. The cyst wall is also heavily stained by the chitin binding lectin succinylated wheat germ agglutinin (s-WGA), which selectively binds to *N*-acetylglucosamine-decorated structures. Here, we tracked the localization of *N*-acetylglucosamine-decorated structures that bind to s-WGA in immature and mature *in vitro* cysts. s-WGA localization was observed at the cyst periphery 6 h after the differentiation of the tachyzoite-stage parasitophorous vacuole. By day 1 and at all later times after differentiation, s-WGA was localized in a continuous staining pattern at the cyst wall. Coinciding with the maturation of the cyst matrix by day 3 of cyst development, s-WGA also localized in a continuous matrix pattern inside the cyst. s-WGA localized in both the outer and inner layer regions of the cyst wall and in a continuous matrix pattern inside mature 7- and 10-day-old cysts. In addition, s-WGA colocalized in the cyst wall with CST1, suggesting that *N*-acetylglucosamine- and *N*-acetylgalactosamine-decorated molecules colocalized in the cyst wall. In contrast to CST1, GRA4, and GRA6, the relative accumulation of the molecules that bind s-WGA in the cyst wall was not dependent on the expression of GRA2. Our results suggest that GRA2-dependent and GRA2-independent mechanisms regulate the trafficking and accumulation of glycosylated molecules that colocalize in the cyst wall.

**IMPORTANCE** Chronic *Toxoplasma gondii* infection is maintained in the central nervous system by thick-walled cysts. If host immunity wanes, cysts recrudesce and cause severe and often lethal toxoplasmic encephalitis. Currently, there are no therapies to eliminate cysts, and little biological information is available regarding cyst structure(s). Here, we investigated cyst wall molecules recognized by succinylated wheat germ agglutinin (s-WGA), a lectin that specifically binds to *N*-acetylglucosamine-decorated structures. *N*-Acetylglucosamine regulates cell signaling and plays structural roles at the cell surface in many organisms. The cyst wall and cyst matrix were heavily stained by s-WGA in mature cysts and were differentially stained during cyst development. The relative accumulation of molecules that bind to s-WGA in the cyst wall was not dependent on the expression of GRA2. Our findings suggest that glycosylated cyst wall molecules gain access to the cyst wall via GRA2-dependent and GRA2-independent mechanisms and colocalize in the cyst wall.

**KEYWORDS** *Toxoplasma gondii*, cysts, chronic infection, cyst wall, cyst matrix, bradyzoite differentiation, cyst development, *N*-acetylglucosamine, s-WGA

*Toxoplasma gondii* is a protozoan pathogen that chronically infects one-third of the global human population (1). Lifelong infection is established by the formation of thick-walled tissue cysts, which mediate parasite transmission (2). Humans are infected by the ingestion of tissue cysts in undercooked meat or oocysts in water or unwashed food (3, 4). *Toxoplasma* infection causes severe ocular infections of the eye (5), and primary infection during pregnancy causes severe congenital defects in the newborn (6,

**Citation** Guevara RB, Fox BA, Bzik DJ. 2020. Succinylated wheat germ agglutinin colocalizes with the *Toxoplasma gondii* cyst wall glycoprotein CST1. *mSphere* 5:e00031-20. <https://doi.org/10.1128/mSphere.00031-20>.

**Editor** Silvia N. J. Moreno, University of Georgia

**Copyright** © 2020 Guevara et al. This is an open-access article distributed under the terms of the [Creative Commons Attribution 4.0 International license](https://creativecommons.org/licenses/by/4.0/).

Address correspondence to David J. Bzik, [david.j.bzik@dartmouth.edu](mailto:david.j.bzik@dartmouth.edu).

**Received** 9 January 2020

**Accepted** 16 February 2020

**Published** 4 March 2020

7). AIDS, cancer, and transplant patients with weakened immunity are susceptible to reactivated chronic infection that causes life-threatening toxoplasmic encephalitis (8, 9). Therapies with the ability to target the cyst stage are not yet available.

During acute infection, tachyzoite-stage parasites replicate within a transient parasitophorous vacuole (PV) that is breached when tachyzoites egress to invade new host cells (10, 11). In chronic infection, bradyzoite-stage parasites reside in a more permanent structure, termed the cyst. While the biology of cyst formation is not yet well understood, prominent cyst structures include the limiting cyst membrane, the cyst wall, and the cyst matrix, which surround the bradyzoite-stage parasites. After tachyzoite-to-bradyzoite-stage differentiation is triggered, the PV membrane (PVM) develops into the cyst membrane (12). A 200- to 850-nm-thick cyst wall forms beneath the cyst membrane (13, 14). Within 6 h after differentiation, cyst wall cargo is already accumulating at the cyst periphery (12, 15). In mature cysts, the cyst wall is organized into two distinct filamentous layers, a more densely compacted outer layer beneath a limiting cyst membrane and a less densely compacted inner layer that faces the cyst matrix (13). The major cyst wall glycoprotein CST1, at least 22 dense granule (GRA) proteins, and other proteins, including CST4, BPK1, MAG1, MCP3, MCP4, and MYR1, were identified in the cyst wall/membrane of *in vitro* cysts (16). In addition, CST1, GRA2, GRA5, GRA6, GRA7, and GRA12 occupy both cyst wall layers, while GRA1, GRA4, and GRA9 occupy only the inner layer of the cyst wall in mature *in vitro* cysts (12, 15). Genetic deletion of cyst membrane- and cyst wall-associated GRA proteins significantly reduced cyst burdens in mice infected with *Toxoplasma* (17–19), suggesting that cyst membrane- and cyst wall-associated GRA proteins were important for the formation and durability of cysts.

The cyst matrix is an intricate environment decorated with soluble components, filamentous materials, vesicles, and membranous tubules (13). The cyst matrix membranous tubules, which also extend into the cyst wall, were previously suggested to be structures that are similar to the intravacuolar network (IVN) membranes characterized in the tachyzoite PV and were therefore named the intracyst network (ICN) (13, 14). A complex of IVN-associated GRAs, GRA2/GRA4/GRA6, interacts with the membranous tubules (20, 21). IVN-associated GRA2 induces the formation of curved tubules from vesicular material secreted from the posterior end of the parasite, and GRA6 stabilizes the curvature of the newly formed membranous tubules (21). The cyst matrix forms 3 days after differentiation and fills the spaces between the bradyzoites and the cyst wall (15). In mature *in vitro* cysts, GRA1, GRA4, GRA6, and GRA9 established a continuous matrix pattern, while GRA2 and GRA12 were isolated in distinct puncta in the cyst matrix (15). GRA2 regulates the development of the cyst wall and the organization of the cyst matrix (15).

Cysts isolated from chronically infected mice were previously assessed with a variety of lectins to identify carbohydrate structures associated with the cyst wall (22–24). The cyst wall is intensely stained by two lectins, *Dolichos biflorus* agglutinin (DBA) and succinylated wheat germ agglutinin (s-WGA) (23, 24). DBA selectively recognizes terminal  $\alpha$ -linked *N*-acetylgalactosamine structures (25). DBA preferentially binds to the mucin domain of CST1, the major cyst wall glycoprotein (19). The CST1-mucin domain is *O*-linked *N*-acetylgalactosamine glycosylated by ppGalNAc-T2 and -T3 (26). Deletion of the *Toxoplasma* nucleotide sugar transporter (TgNST1) ablated cyst wall recognition by DBA as well as s-WGA (27), suggesting that *Toxoplasma* steals nucleotide sugars from the host cell. A second *O*-linked glycosylated mucin domain-containing cyst wall glycoprotein was recently identified as SRS13 (28). However, SRS13 is a low-abundance cyst wall protein (16), which is consistent with the observation that DBA staining of the cyst wall was abolished in cysts that lacked the expression of CST1 (19). Genetic deletion of CST1 reduced the number of brain cysts, and these CST1-deficient cysts exhibited a fragile-cyst phenotype characterized by a thin cyst wall and cysts that were easily disrupted by mechanical force (19).

In contrast to the *N*-acetylgalactosamine specificity of DBA, the chitin binding lectin s-WGA selectively binds to *N*-acetylglucosamine-modified structures (29). Lectin overlay

experiments previously revealed that s-WGA selectively recognized an ~48-kDa cyst wall-localized glycoprotein that is not related to CST1 (23). Treatment of *Toxoplasma* cysts with chitinase, an enzyme specific for a  $\beta$ -1,4-linked polymer of *N*-acetylglucosamine, degraded the cyst wall and released bradyzoites (24, 30). In addition, s-WGA failed to stain the cyst wall of cysts that were pretreated with chitinase (24). Together, these observations suggested that s-WGA binds to an *N*-acetylglucosamine-modified glycoprotein that is essential for the stability of the cyst wall.

Exposure of tachyzoite PVs to low CO<sub>2</sub> and high pH triggers tachyzoite-to-bradyzoite differentiation (31, 32), and this *in vitro* differentiation method can produce mature, orally infectious cysts (33) that possess the characteristic cyst structures of *in vivo* cysts isolated from brains of infected mice (34). Here, we investigated s-WGA staining of cysts to (i) localize the *N*-acetylglucosamine-modified molecules that bind s-WGA during cyst development and (ii) test whether the accumulation of the s-WGA-binding *N*-acetylglucosamine-modified molecules in the cyst wall is regulated by GRA2. Our results show that s-WGA recognized *N*-acetylglucosamine-modified molecules at the cyst periphery/wall throughout cyst development and in the cyst matrix by day 3 after differentiation. The deletion of GRA2 did not affect the trafficking or cyst wall accumulation of the molecules that bind s-WGA in the cyst wall, and the cyst wall molecule(s) that binds s-WGA was colocalized with GRA4, GRA6, and CST1.

## RESULTS

**s-WGA localizes to the cyst wall and cyst matrix during cyst development.** The lectin s-WGA selectively recognizes an unidentified ~48-kDa cyst wall glycoprotein (23). We used a streptavidin-biotin labeling scheme to track s-WGA localization during cyst development. Since streptavidin was previously observed to label endogenously biotinylated proteins in the apicoplast of tachyzoite-stage parasites (35–37), we performed control experiments to determine whether bradyzoite apicoplast biotin was detected. While the bradyzoite apicoplast was detected in cysts that were labeled only with streptavidin (see Fig. S1A in the supplemental material), the bradyzoite apicoplast was not detected in cysts that were initially stained with biotinylated s-WGA and then subsequently stained with streptavidin (Fig. S1B). Using this modified labeling scheme, we tracked the locations of the *N*-acetylglucosamine-modified molecules that bind to s-WGA in 6-h-, 1-day-, 2-day-, 3-day-, 7-day-, and 10-day-old *in vitro* cysts. Green fluorescent protein-positive (GFP<sup>+</sup>) bradyzoites were visible within developing cysts (Fig. 1). s-WGA staining was observed by as early as 6 h and at all later times of cyst development. The s-WGA staining patterns indicated that (i) at 6 h, s-WGA staining was observed as puncta at the cyst periphery; (ii) at 1 and 2 days, s-WGA was continuous around the cyst periphery; (iii) at 3 days, s-WGA was at the cyst periphery and visibly stained the cyst matrix; and (iv) at 7 and 10 days, s-WGA was at the cyst wall and established a continuous matrix pattern in the cyst (Fig. 1). In 7- and 10-day-old mature cysts, the cyst wall was visualized as a distinct structure by differential interference contrast (DIC) microscopy (Fig. 1). These observations suggested that the *N*-acetylglucosamine-modified molecules recognized by s-WGA were expressed early in the developing cyst and were associated with the cyst periphery/wall and cyst matrix during cyst development and cyst maturation.

**The localization of s-WGA in immature cysts is not dependent on GRA2 expression.** The relative accumulation of GRA4, GRA6, and CST1 at the cyst periphery/wall was delayed in  $\Delta gra2$  cysts (15). To measure whether the relative accumulation of the *N*-acetylglucosamine-modified molecules that bind to s-WGA at the cyst periphery/wall was also regulated by GRA2, immature cysts were differentiated for 1 day, 2 days, or 3 days, and s-WGA colocalization with GRA4 (Fig. 2) or GRA6 (Fig. 3) was assessed in parental Pru $\Delta ku80$  and  $\Delta gra2$  cysts that lacked the expression of GRA2 (Fig. S1B). GFP<sup>+</sup> bradyzoites were visible in s-WGA-stained cysts. In 1- and 2-day-old Pru $\Delta ku80$  cysts, s-WGA preferentially localized at the cyst periphery and colocalized with GRA4 (Fig. 2A and B) and GRA6 (Fig. 3A and B). In contrast, in 1- and 2-day-old  $\Delta gra2$  cysts, s-WGA weakly colocalized at the cyst periphery with GRA4 and GRA6. In 3-day-old Pru $\Delta ku80$

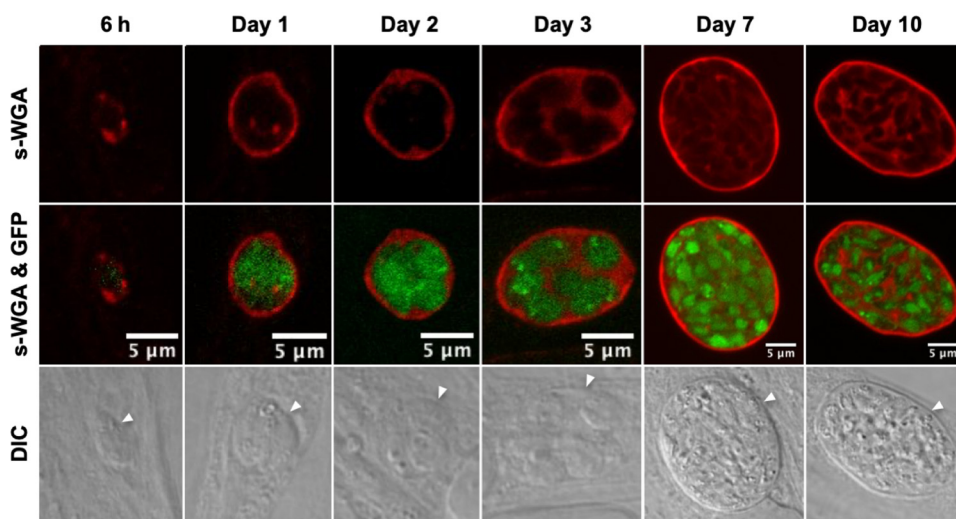


**FIG 1** s-WGA lectin stains the cyst periphery, cyst wall, and cyst matrix throughout cyst development. *In vitro* cysts derived from the parental *Prudku80* strain were differentiated for 6 h, 1 day, 2 days, 3 days, 7 days, or 10 days. Cysts were located using differential interference contrast (DIC) microscopy and imaged by confocal microscopy. The presence of bradyzoites inside cysts was verified by locating parasite nuclei with 4',6-diamidino-2-phenylindole (DAPI) staining (not shown) and verifying that each parasite nucleus was surrounded by the expression of cytosolic GFP (GFP<sup>+</sup> bradyzoites). Cysts were stained with biotinylated s-WGA. Panels show s-WGA, s-WGA and GFP, and DIC (cyst walls are indicated by white arrowheads). The number of cysts analyzed was 8 to 20. Representative images are shown.

cysts, s-WGA colocalized at the cyst periphery and also in the cyst matrix with GRA4 (Fig. 2C) and GRA6 (Fig. 3C), and this colocalization was reduced in  $\Delta gra2$  cysts. In 3-day-old *Prudku80* cysts, GRA4 (Fig. 2C) and GRA6 (Fig. 3C) also exhibited a continuous matrix staining pattern that transitioned to a less continuous punctum-speckled matrix pattern in  $\Delta gra2$  cysts. In contrast, s-WGA displayed a continuous matrix pattern in both *Prudku80* and  $\Delta gra2$  cysts.

To quantify the location of s-WGA, GRA4, and GRA6 in immature cysts, we measured the fluorescence intensity at the cyst periphery relative to that at the cyst interior using a Fiji macro (15). While the cyst periphery/cyst interior ratios of GRA4 (Fig. 2D to F) and GRA6 (Fig. 3D to F) were significantly reduced in  $\Delta gra2$  cysts compared to parental *Prudku80* cysts, the lack of GRA2 expression did not affect the s-WGA cyst periphery/cyst interior ratio. In addition, the cyst periphery/cyst interior fluorescence intensity ratios of GRA4 (Fig. 2D and E), GRA6 (Fig. 3D and E), and s-WGA (Fig. 2D and E and Fig. 3D and E) were  $>1.0$  in 1- and 2-day-old cysts, indicating that these molecules were preferentially localized in the cyst wall early in cyst development (15). Compared to 1- and 2-day-old cysts, the cyst periphery/cyst interior fluorescence intensity ratios of GRA4 (Fig. 2F), GRA6 (Fig. 3F), and s-WGA (Fig. 2F and Fig. 3F) were decreased in 3-day-old cysts, indicating that these molecules were also prominent in the cyst matrix by day 3 of cyst development.

To quantitatively assess the location(s) of GRA4, GRA6, and s-WGA, we measured the cyst fluorescence intensity profiles of GRA4 and GRA6 relative to s-WGA using the Fiji macro (15). The fluorescence intensity peaks of GRA4 (Fig. S2A to C) and GRA6 (Fig. S2D to F) overlapped that of s-WGA, indicating their presence at the cyst periphery in *Prudku80* cysts. In contrast, in  $\Delta gra2$  cysts, the fluorescence intensity peaks of GRA4 and GRA6 were shifted to the right (cyst matrix) of the s-WGA peak, confirming a reduced localization of GRA4 (Fig. S2A to C) and GRA6 (Fig. S2D to F) in the  $\Delta gra2$  cyst wall (15). However, the fluorescence intensity of s-WGA at the cyst periphery/wall was not affected in 1-, 2-, or 3-day-old  $\Delta gra2$  cysts.

**The localization of s-WGA in mature cysts is not dependent on GRA2 expression.** Mature cysts were differentiated for 7 days or 10 days, and the colocalization of s-WGA with GRA4 (Fig. 4) or GRA6 (Fig. 5) was measured. GFP<sup>+</sup> bradyzoites were visible

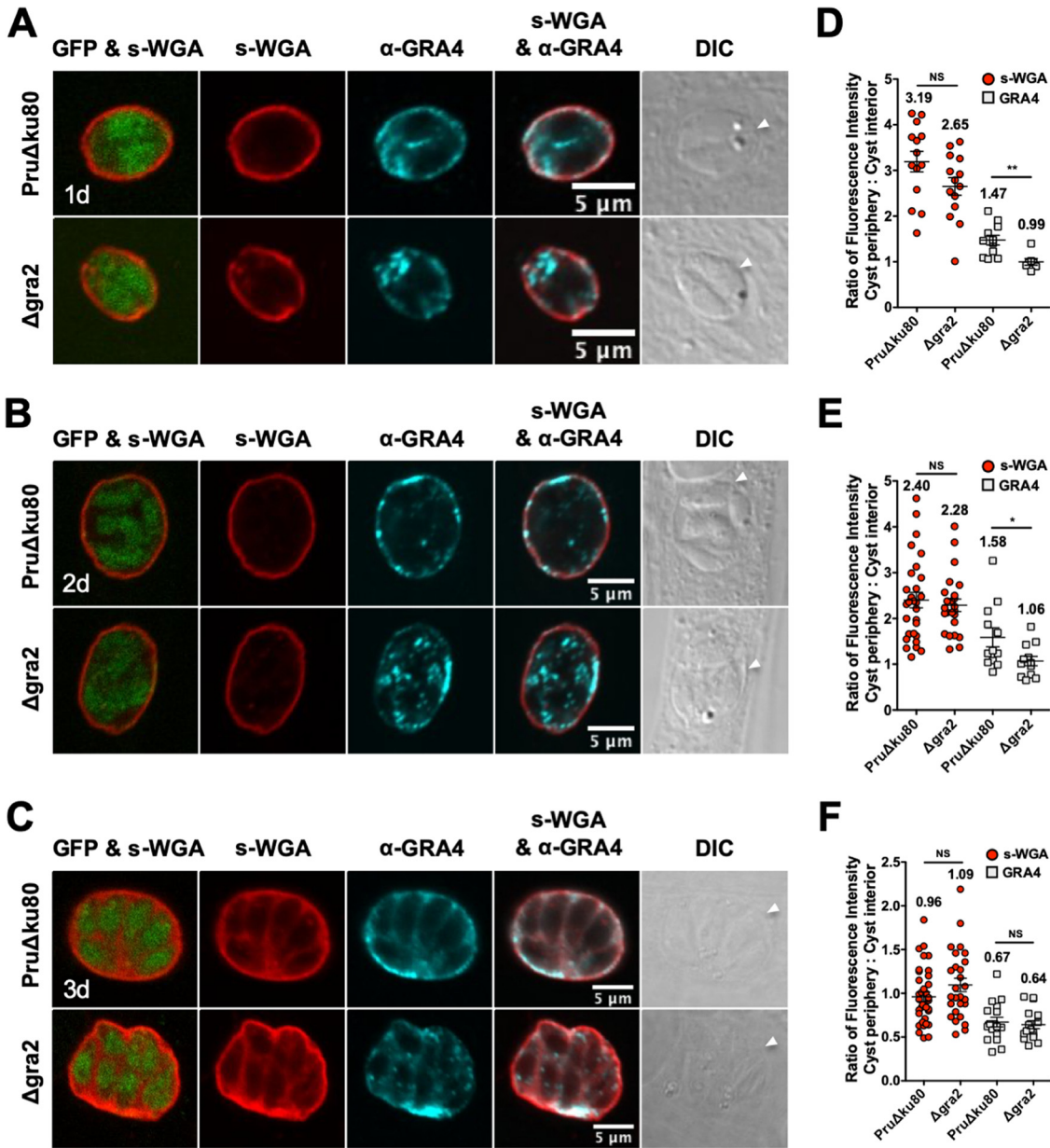


**FIG 2** s-WGA colocalizes with GRA4 at the cyst periphery, and s-WGA accumulation at the cyst periphery is GRA2 independent in immature cysts. *PruΔku80*- and *Δgra2*-infected human foreskin fibroblast (HFF) cells on coverslips were treated under bradyzoite-inducing conditions to differentiate *in vitro* cysts for 1 day, 2 days, or 3 days. Cysts were located using DIC microscopy and imaged by confocal microscopy. (A to C) The presence of bradyzoites inside cysts was verified by locating parasite nuclei with DAPI staining (not shown) and verifying that each parasite nucleus was surrounded by the expression of cytosolic GFP (GFP<sup>+</sup> bradyzoites). Cysts were stained with biotinylated s-WGA and anti-GRA4 antibody. Panels show GFP and s-WGA, s-WGA, anti-GRA4, s-WGA and anti-GRA4, and DIC (cyst walls are indicated by white arrowheads). s-WGA colocalized with GRA4 in 100% of cysts evaluated at day 1 ( $n = 11$ ) (A), day 2 ( $n = 12$ ) (B), and day 3 ( $n = 17$ ) (C). (D to F) Fluorescence intensities of s-WGA and GRA4 were measured at the cyst periphery and within the cyst (cyst interior) in *PruΔku80* and *Δgra2* cysts at day 1 (D), day 2 (E), and day 3 (F). Data are plotted as the ratio of the mean fluorescence intensity at the cyst periphery to that within the cyst interior  $\pm$  SEM. The numbers of cysts analyzed for the parental *PruΔku80* and *Δgra2* strains for s-WGA and GRA4 are as follows: s-WGA ( $n = 14$ ,  $n = 14$  cysts) and GRA4 ( $n = 11$ ,  $n = 7$  cysts) at day 1 (D), s-WGA ( $n = 29$ ,  $n = 24$  cysts) and GRA4 ( $n = 12$ ,  $n = 12$  cysts) at day 2 (E), and s-WGA ( $n = 36$ ,  $n = 27$  cysts) and GRA4 ( $n = 17$ ,  $n = 16$  cysts) at day 3 (F). The numerical ratio for the mean fluorescence intensity is labeled for s-WGA and GRA4.  $P$  values were calculated using Student's  $t$  test (\*,  $P < 0.05$ ; \*\*,  $P < 0.01$ ; NS, not significant).

in s-WGA-stained cysts. In parental *PruΔku80* cysts, GRA4 (Fig. 4A and B) and GRA6 (Fig. 5A and B) colocalized with s-WGA at the cyst wall as well as in a continuous matrix pattern in the cyst matrix. This colocalization pattern was markedly reduced in *Δgra2* cysts. The cyst periphery/cyst interior fluorescence intensity ratios of s-WGA (0.48)

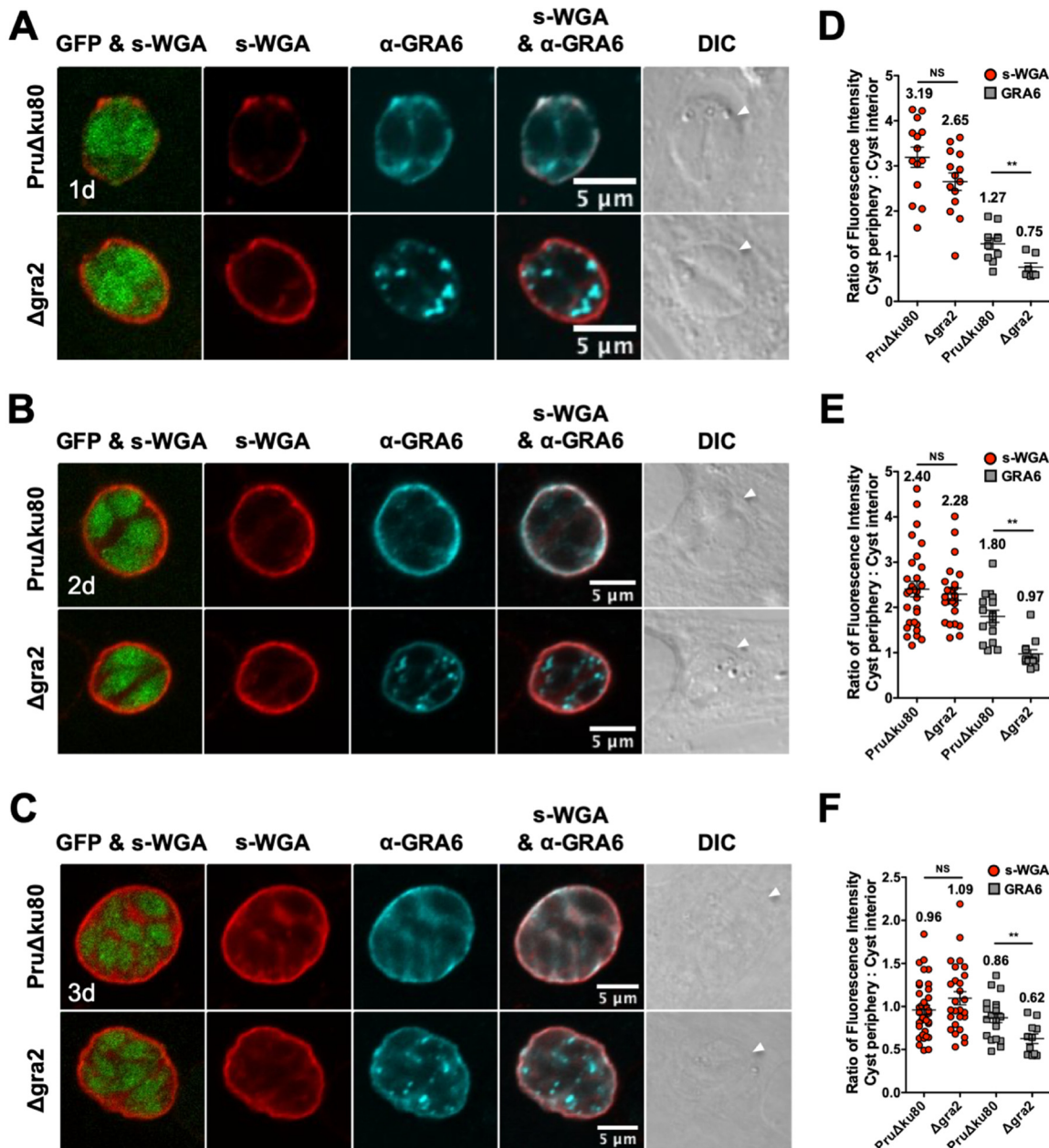


**FIG 3** s-WGA colocalizes with GRA6 at the cyst periphery, and s-WGA accumulation at the cyst periphery is GRA2 independent in immature cysts. *PruΔku80*- and *Δgra2*-infected HFF cells on coverslips were treated under bradyzoite-inducing conditions to differentiate *in vitro* cysts for 1 day, 2 days, or 3 days. Cysts were located using DIC microscopy and imaged by confocal microscopy. (A to C) The presence of bradyzoites inside cysts was verified by locating parasite nuclei with DAPI staining (not shown) and verifying that each parasite nucleus was surrounded by the expression of cytosolic GFP (GFP<sup>+</sup> bradyzoites). Cysts were stained with biotinylated s-WGA and anti-GRA6 antibody. Panels show GFP and s-WGA, s-WGA, anti-GRA6, s-WGA and anti-GRA6, and DIC (cyst walls are indicated by white arrowheads). s-WGA was colocalized with GRA6 in 100% of cysts evaluated at day 1 (*n* = 10) (A), day 2 (*n* = 16) (B), and day 3 (*n* = 19) (C). (D to F) Fluorescence intensities of s-WGA and GRA6 were measured at the cyst periphery and within the cyst (cyst interior) in *PruΔku80* and *Δgra2* cysts at day 1 (D), day 2 (E), and day 3 (F). Data are plotted as the ratio of the mean fluorescence intensity at the cyst periphery to that within the cyst interior ± SEM. The numbers of cysts analyzed for the parental *PruΔku80* and *Δgra2* strains for s-WGA and GRA6 are as follows: s-WGA (*n* = 14, *n* = 14 cysts) and GRA6 (*n* = 10, *n* = 7 cysts) at day 1 (D), s-WGA (*n* = 29, *n* = 24 cysts) and GRA6 (*n* = 16, *n* = 12 cysts) at day 2 (E), and s-WGA (*n* = 36, *n* = 27 cysts) and GRA6 (*n* = 19, *n* = 11 cysts) at day 3 (F). The numerical ratio for the mean fluorescence intensity is labeled for s-WGA and GRA6. *P* values were calculated using Student's *t* test (\*\*, *P* < 0.01; NS, not significant).

(Fig. 4C and Fig. 5C), GRA4 (0.52) (Fig. 4C), and GRA6 (0.54) (Fig. 5C) were similar in parental *PruΔku80* 7-day-old cysts, indicating cyst wall and cyst matrix localizations (15). The fluorescence intensity ratios of GRA4 (0.48) (Fig. 4D) and GRA6 (0.58) (Fig. 5D) in 10-day-old cysts remained similar to those in 7-day-old cysts, whereas the s-WGA ratio

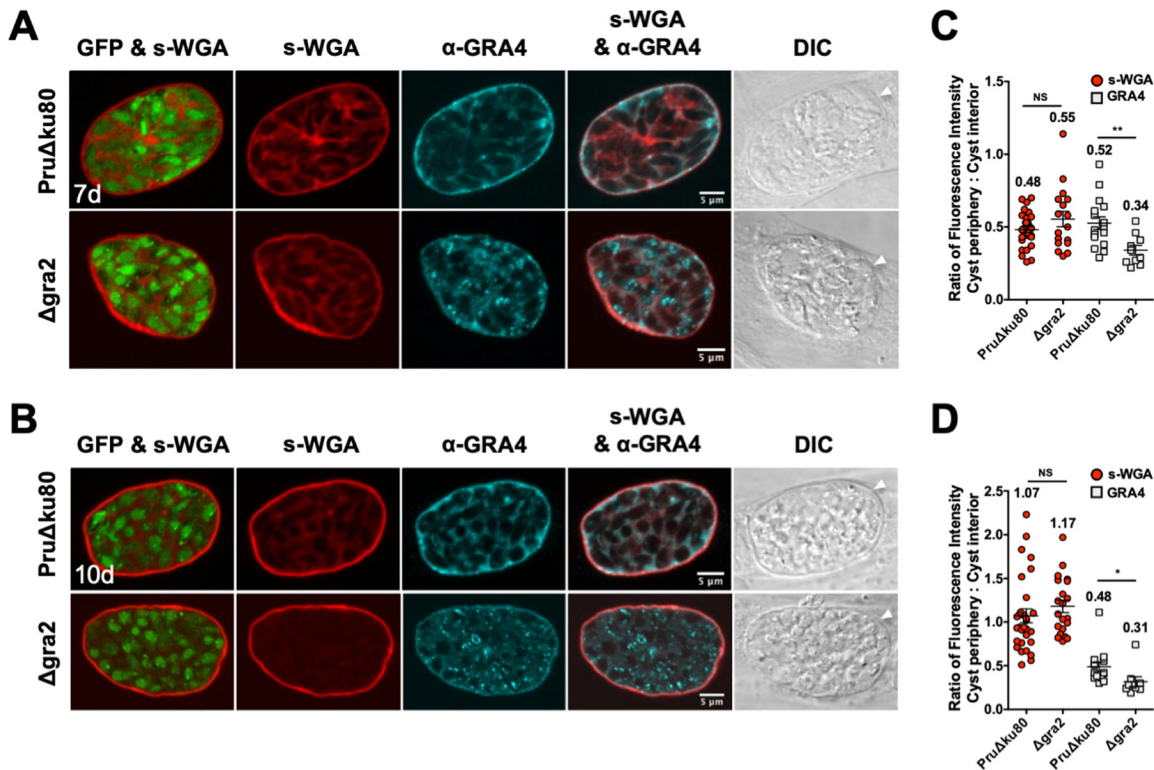


**FIG 4** s-WGA colocalizes with GRA4 at the cyst periphery, and s-WGA accumulation at the cyst periphery is GRA2 independent in mature cysts. PruDku80- and Δgra2-infected HFF cells were treated under bradyzoite-inducing conditions to differentiate *in vitro* cysts for 7 days or 10 days. Cysts were located using DIC microscopy and imaged by confocal microscopy. (A and B) The presence of bradyzoites inside cysts was verified by locating parasite nuclei with DAPI staining (not shown) and verifying that each parasite nucleus was surrounded by the expression of cytosolic GFP (GFP<sup>+</sup> bradyzoites). Cysts were stained with biotinylated s-WGA and anti-GRA4 antibody. Panels show GFP and s-WGA, s-WGA, anti-GRA4, s-WGA and anti-GRA4, and DIC (cyst walls are indicated by white arrowheads). s-WGA was colocalized with GRA4 in 100% of cysts evaluated at day 7 ( $n = 16$ ) (A) and day 10 ( $n = 14$ ) (B). (C and D) Fluorescence intensities of s-WGA and GRA4 were measured at the cyst periphery and within the cyst (cyst interior) in PruDku80 and Δgra2 cysts. Data are plotted as the ratio of the mean fluorescence intensity at the cyst periphery to that within the cyst interior  $\pm$  SEM. The numbers of cysts analyzed for the parental PruDku80 and Δgra2 strains for s-WGA and GRA4 are as follows: s-WGA ( $n = 31$ ,  $n = 17$  cysts) and GRA4 ( $n = 16$ ,  $n = 10$  cysts) at day 7 (C), and s-WGA ( $n = 30$ ,  $n = 21$  cysts) and GRA4 ( $n = 14$ ,  $n = 9$  cysts) at day 10 (D). The numerical ratio for the mean fluorescence intensity is labeled for s-WGA and GRA4.  $P$  values were calculated using Student's  $t$  test (\*,  $P < 0.05$ ; \*\*,  $P < 0.01$ ; NS, not significant).

(Fig. 4D and Fig. 5D) was increased to 1.07, indicating the accumulation of s-WGA binding molecules in the cyst wall of 10-day-old cysts. In contrast to GRA4 and GRA6, the cyst periphery/cyst interior fluorescence intensity ratio of s-WGA was not affected in Δgra2 cysts. The fluorescence intensity peak of GRA4 (Fig. S3A and B) was shifted toward the cyst matrix in comparison to s-WGA. In contrast, the GRA6 (Fig. S3C and D) peak overlapped that of s-WGA, suggesting that s-WGA, like GRA6, was present in all layers of the cyst wall, whereas GRA4 primarily occupies the inner layers of the cyst wall.

**s-WGA colocalizes with CST1 in the cyst wall.** We detected the colocalization of s-WGA binding molecules in the cyst wall with GRA4 and GRA6 in immature and mature cysts. To investigate the localization of s-WGA in relation to the major cyst wall protein CST1, we differentiated cysts for 3, 7, or 10 days and determined the localizations of s-WGA and CST1. Nuclei stained with 4',6-diamidino-2-phenylindole (DAPI) were visible inside GFP<sup>+</sup> bradyzoites (Fig. 6). As expected, CST1 localized to the cyst wall, while s-WGA localized to the cyst periphery/wall as well as to the cyst matrix in immature 3-day-old cysts and in mature 7- and 10-day-old cysts. Colocalization of CST1 and s-WGA was detected at the cyst periphery (Fig. 6A). To confirm that CST1 and s-WGA were colocalized in the cyst wall, we measured the cyst fluorescence intensity profiles for CST1 and s-WGA. CST1 was present in all layers of the cyst wall and colocalized with s-WGA in 3-day-old (Fig. 6B), 7-day-old (Fig. 6C), and 10-day-old (Fig. 6D) cysts. We quantitatively measured CST1 and s-WGA fluorescence intensities at the cyst periphery

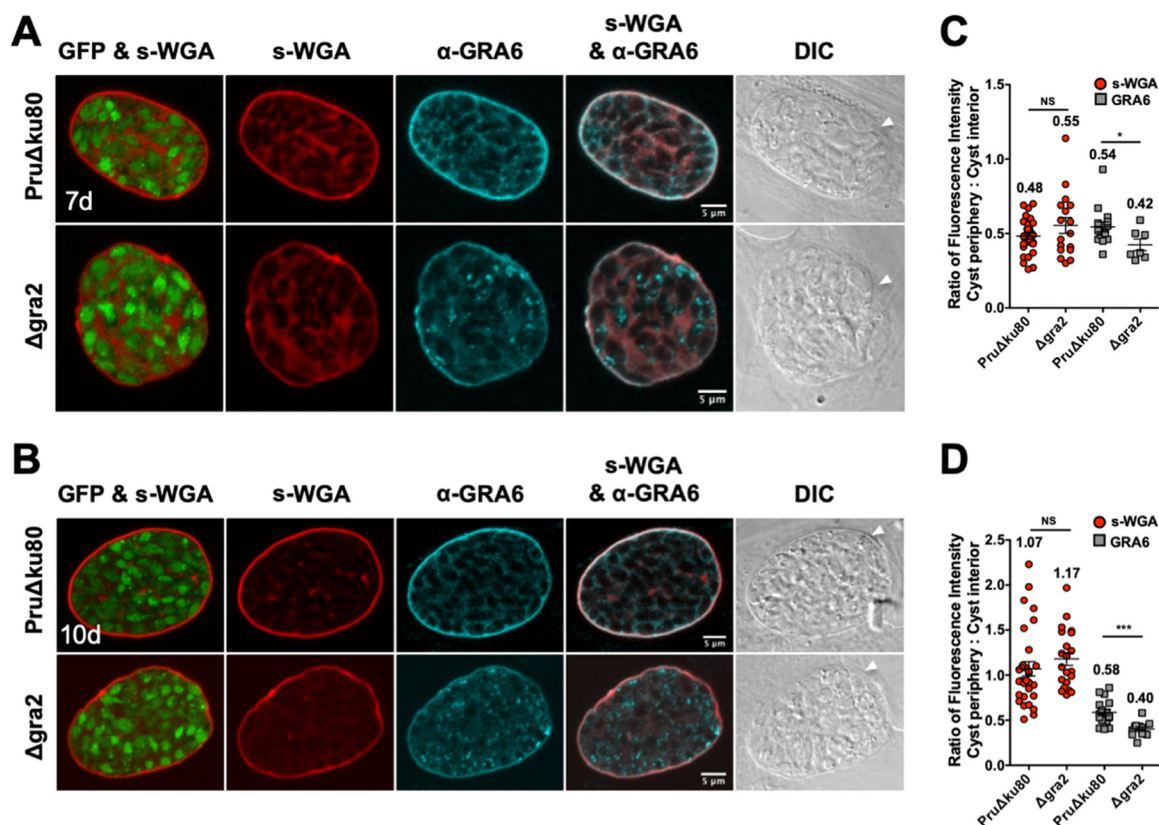


**FIG 5** s-WGA colocalizes with GRA6 at the cyst periphery, and s-WGA accumulation at the cyst periphery is GRA2 independent in mature cysts. *PruΔku80*- and *Δgra2*-infected HFF cells were treated under bradyzoite-inducing conditions to differentiate *in vitro* cysts for 7 days or 10 days. Cysts were located using DIC microscopy and imaged by confocal microscopy. (A and B) The presence of bradyzoites inside cysts was verified by locating parasite nuclei with DAPI staining (not shown) and verifying that each parasite nucleus was surrounded by the expression of cytosolic GFP (GFP<sup>+</sup> bradyzoites). Cysts were stained with biotinylated s-WGA and anti-GRA6 antibody. Panels show GFP and s-WGA, s-WGA, anti-GRA6, s-WGA and anti-GRA6, and DIC (cyst walls are indicated by white arrowheads). s-WGA was colocalized with GRA6 in 100% of cysts evaluated at day 7 ( $n = 15$ ) (A) and day 10 ( $n = 16$ ) (B). (C and D) Fluorescence intensities of s-WGA and GRA6 were measured at the cyst periphery and within the cyst (cyst interior) in *PruΔku80* and *Δgra2* cysts. Data are plotted as the ratio of the mean fluorescence intensity at the cyst periphery to that within the cyst interior  $\pm$  SEM. The numbers of cysts analyzed for the parental *PruΔku80* and *Δgra2* strains for s-WGA and GRA6 are as follows: s-WGA ( $n = 31$ ,  $n = 17$  cysts) and GRA6 ( $n = 15$ ,  $n = 7$  cysts) at day 7 (C), and s-WGA ( $n = 30$ ,  $n = 21$  cysts) and GRA6 ( $n = 16$ ,  $n = 12$  cysts) at day 10 (D). The numerical ratio for the mean fluorescence intensity is labeled for s-WGA and GRA6.  $P$  values were calculated using Student's  $t$  test (\*,  $P < 0.05$ ; \*\*\*,  $P < 0.005$ ; NS, not significant).

compared to those at the cyst interior. While CST1 was preferentially localized to the cyst wall (cyst periphery/cyst interior ratio of  $>1.0$ ), the *N*-acetylglucosamine-modified molecules that bind s-WGA were present in the cyst wall and in the cyst matrix (cyst periphery/cyst interior ratio of  $<1.0$ ) (Fig. 6E).

## DISCUSSION

Protozoan parasites possess survival strategies to maintain viability inside and outside the host(s) by forming cyst structures (38, 39). Neurons are the primary target cells for *Toxoplasma* cyst formation within distal neuronal processes (40, 41). Bradyzoite differentiation is triggered by changes in nutrition or cellular conditions (42–44), which drives the transcriptional program that leads to the production of bradyzoite-stage proteins (45, 46) and the formation of the cyst wall and cyst structure (32). The cyst wall is a protective structure that safely encloses bradyzoites until their transmission to a new host after oral ingestion of cysts (14). Glycosylated proteins are a major component of the cyst wall (19), which is an obstacle for cyst clearance and elimination by the host (47).

Tachyzoite-to-bradyzoite differentiation is linked with major changes in carbohydrate and polysaccharide metabolism (38, 48, 49). The *Toxoplasma* cyst wall is recognized by a variety of lectins, including concanavalin A ( $\alpha$ -D-mannose or  $\alpha$ -D-glucose),



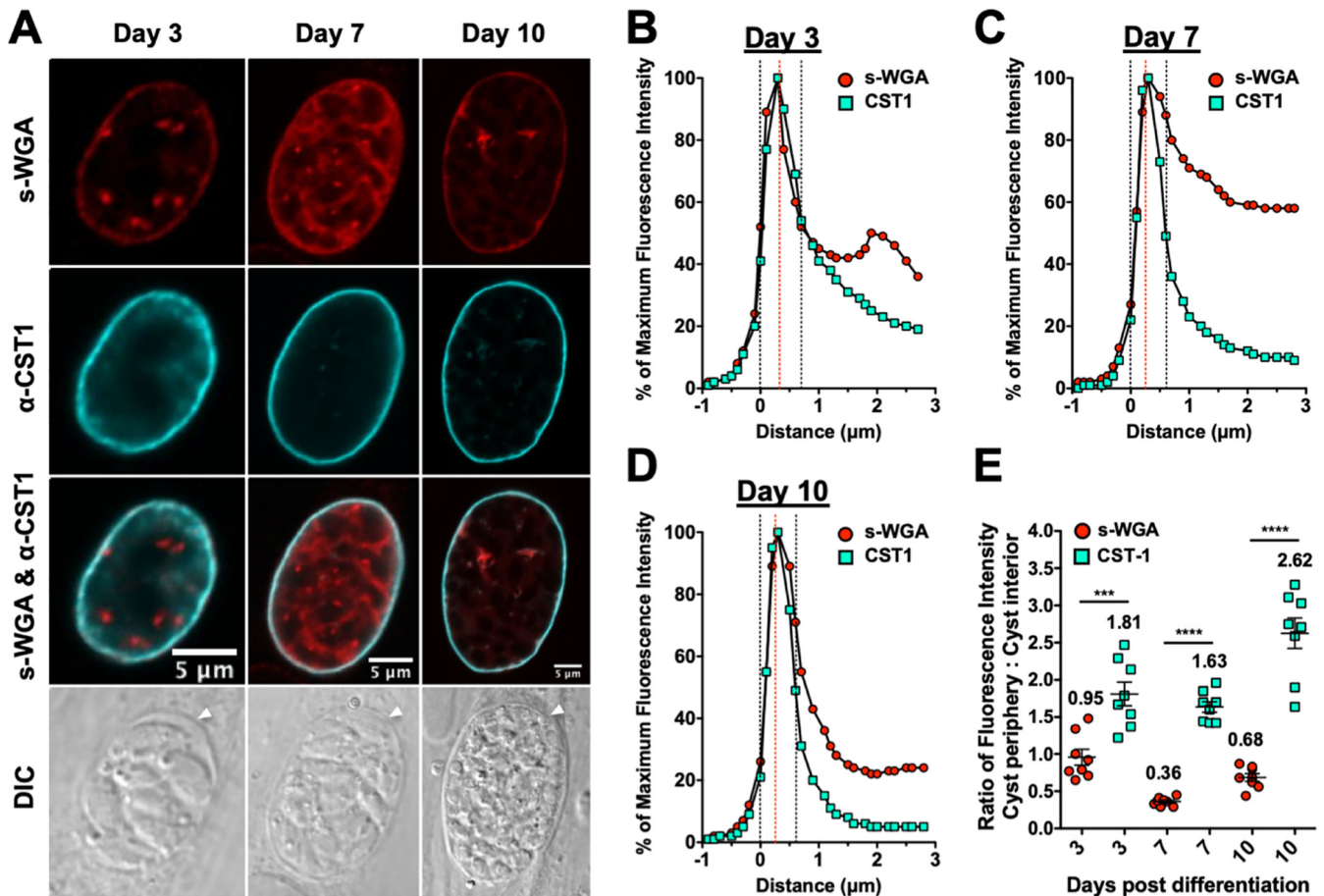


**FIG 6** s-WGA colocalizes with CST1 at the cyst wall. PruΔku80-infected HFF cells were treated under bradyzoite-inducing conditions to differentiate *in vitro* cysts for 3 days, 7 days, or 10 days. Cysts were located using DIC microscopy and imaged by confocal microscopy. (A) The presence of bradyzoites inside cysts was verified by locating parasite nuclei with DAPI staining and verifying that each parasite nucleus was surrounded by the expression of cytosolic GFP (GFP<sup>+</sup> bradyzoites) (not shown). Cysts were stained with biotinylated s-WGA and anti-CST1 antibody. Panels show GFP and DAPI, s-WGA, anti-CST1, s-WGA and anti-CST1, and DIC (cyst walls are indicated by white arrowheads). s-WGA was colocalized with CST1 at 3 days ( $n = 8$ ), 7 days ( $n = 8$ ), or 10 days ( $n = 8$ ) in 100% of cysts evaluated. (B to D) Fluorescence intensity profiles of representative cysts shown in panel A were generated to quantify the location of s-WGA relative to the cyst wall as shown by CST1 at day 3 (B), day 7 (C), and day 10 (D). Dotted black lines define the cyst wall region. The dotted red line indicates the middle of the cyst wall. (E) Fluorescence intensities of s-WGA and CST1 were measured at the cyst periphery and within the cyst (cyst interior) at day 3, day 7, and day 10. Data are plotted as the ratio of the mean fluorescence intensity at the cyst periphery to that within the cyst interior  $\pm$  SEM ( $n = 8$  cysts). The numerical ratio for the mean fluorescence intensity is labeled for s-WGA and CST1 for each day shown.  $P$  values were calculated using Student's  $t$  test (\*\*\*,  $P < 0.005$ ; \*\*\*\*,  $P < 0.0001$ ).

wheat germ agglutinin (WGA) (*N*-acetylglucosamine or sialic acid), succinylated WGA (s-WGA) (*N*-acetylglucosamine), soybean agglutinin ( $\alpha$ -helix- or  $\beta$ -sheet-linked *N*-acetyl-D-galactosamine or galactose), and *Dolichos biflorus*, *Vicia villosa*, *Artocarpus integrifolia*, and *Helix pomatia* agglutinins (*N*-acetylglactosamine) (22, 24, 26). The most widely used cyst wall stain is *Dolichos biflorus* agglutinin (DBA), which intensely stains the cyst wall of *in vitro* (31) and *in vivo* (15, 19, 23, 50–52) cysts. DBA selectively recognizes *O*-linked *N*-acetylglactosamine glycosylation of the CST1 mucin domain (19). *O*-linked glycosylation of CST1 is essential for establishing cyst wall thickness and cyst stability (19, 23). *N*-Acetylglactosamine-modified CST1 has been hypothesized to be a key cyst wall scaffolding molecule that interacts with other cyst wall proteins to provide a walled structure that supports cyst stability (13, 53). Our results show that the cyst wall-glycosylated molecule(s) that binds s-WGA colocalized with CST1 in the cyst wall. Together, *N*-acetylglactosamine-modified CST1- and *N*-acetylglucosamine-modified s-WGA-interacting molecules may coordinate the scaffolding and building of the cyst wall.

Bright s-WGA-stained puncta were visible at the cyst periphery in 6-h-differentiated

cysts, suggesting that *N*-acetylglucosamine-modified molecules preferentially accumulated at the cyst periphery/wall early after differentiation. This phenotype mirrors the recent phenotypes that we reported for DBA-stained cyst wall glycoprotein(s) (CST1) and the cyst wall components GRA1, GRA2, GRA4, GRA5, GRA6, GRA7, GRA9, and GRA12 (12, 15). The bright puncta present at the cyst periphery 6 h after differentiation may mark the presence of vesicles secreted by bradyzoites that carry cyst wall cargo for wall building to the cyst periphery. The actin cytoskeleton and Rab11 traffic vesicles to the cyst walls of *Giardia* and *Entamoeba*, supporting a model whereby cyst wall proteins are transported through the cytoskeleton (54, 55). In addition, the *Giardia* Rho GTPase Rac regulates endomembrane organization and cyst wall protein trafficking in *Giardia* (56). How *Toxoplasma* cyst wall cargo for cyst wall building is delivered to the cyst periphery is currently unknown. Future studies with electron and high-resolution microscopy are needed to identify the mechanisms that could traffic cyst wall cargo to the cyst wall.

After differentiation is triggered, the initial tachyzoite-stage PVM develops into the limiting cyst membrane (12). The limiting cyst membrane is ruffled (13, 16, 19). Cyst wall proteins accumulate at the cyst periphery during cyst wall development and localize in the cyst wall beneath the limiting cyst membrane (12, 15). The cyst wall structure has a densely compacted outer layer and a less densely compacted inner layer that faces the cyst matrix and is filled with vesicles and membrane tubules (13). The fluorescence intensity peak of s-WGA overlapped that of CST1, the major cyst wall glycoprotein that is localized throughout the cyst wall (15, 19, 23). Thus, the *N*-acetylglucosamine-modified molecules that bind to s-WGA are present throughout the cyst wall. Furthermore, s-WGA was preferentially localized in the cyst wall early after differentiation at 6 h, 1 day, and 2 days of cyst development. These results support the hypothesis that *N*-acetylglucosamine-modified molecules that bind to s-WGA and colocalize with CST1 play a role in the development and structure of the cyst wall. Genetic deletion of CST1 results in a leaky-cyst phenotype marked by the escape of cyst matrix proteins from the cyst (53), which supports the previously proposed model that *O*-linked *N*-acetylgalactosamine glycosylation regulates the permeability of the cyst wall. It is tempting to speculate that *N*-acetylgalactosamine-modified CST1- and *N*-acetylglucosamine-modified s-WGA binding molecules together establish permeability conduits in the cyst wall that allow the permeation of small essential host molecules such as glucose (57) and nucleotide sugars (27) and, perhaps, vesicular traffic. Additional studies are necessary to identify the structures formed by colocalized CST1- and s-WGA-binding molecules in the cyst wall.

The genetic deletion of GRA2 disrupted the organization of the cyst matrix, altered the staining patterns of GRA4 and GRA6 in the cyst matrix, and delayed the accumulation of GRA4, GRA6, and DBA-stained CST1 in the cyst wall (15). In the tachyzoite-stage PV, GRA2 tubulates vesicles into highly curved membranes, the intravacuolar network (IVN), that connect tachyzoites to one another and to the PVM (21, 58, 59). Similar highly curved membranes, the intracyst network (ICN), are also visible in the cyst matrix and in the cyst wall and connect the bradyzoites to one another and to the cyst wall (13, 14). While s-WGA preferentially stained the cyst wall early after differentiation prior to the formation of the cyst matrix, s-WGA prominently stained both the cyst wall and the cyst matrix of 3-, 7-, and 10-day-old cysts. s-WGA colocalized with GRA4 and GRA6 in the cyst matrix and with GRA4, GRA6, and CST1 in the cyst wall. In contrast to GRA4, GRA6, and DBA-stained CST1 (15), the deletion of GRA2 did not affect s-WGA localization in the cyst matrix or in the cyst wall. Thus, while s-WGA colocalized with GRA4, GRA6, and CST1, which traffic to the cyst wall via a GRA2-dependent pathway (15), the *N*-acetylglucosamine-modified molecule(s) that binds s-WGA traffics to and accumulates at the cyst wall through GRA2-independent mechanisms.

Glycan modifications in the tachyzoite stage have been previously reported to regulate invasion, O<sub>2</sub> sensing, nutrient storage, and *in vitro* growth (60). Skp1 is required for cytoplasmic glycosylation and optimal oxygen-dependent growth (61, 62). Spy (TGME49\_273500) (63) is an enzyme similar to *O*-linked *N*-acetylglucosamine transferase (OGT) that mediates *O*-linked  $\beta$ -*N*-acetylglucosaminylation. *O*-linked  $\beta$ -*N*-

acetylglucosamylation is a posttranslational modification of cytosolic, nuclear, and mitochondrial proteins by a single residue of *N*-acetylglucosamine which is transferred from UDP-*N*-acetylglucosamine and is hypothesized to be involved in the localization of nuclear proteins (64, 65). *O*-linked  $\beta$ -*N*-acetylglucosamylation is reversible by *O*-linked  $\beta$ -*N*-acetylglucosaminyl hydrolase (OGA), which removes the *N*-acetylglucosamine residue (66). *O*-linked  $\beta$ -*N*-acetylglucosamylation levels are dependent on nutritional status (67), and since starvation triggers the tachyzoite-to-bradyzoite transition (42), it is postulated that *O*-linked *N*-acetylglucosamine glycosylation levels would be increased in bradyzoites. In the tachyzoite stage, a variety of *Toxoplasma* proteins are modified with *N*-acetylglucosamine (65), and the tachyzoite proteome of *O*-linked  $\beta$ -*N*-acetylglucosamylation was recently determined (68). s-WGA binds to many tachyzoite-stage-expressed proteins that are glycosylated via *O*-linked *N*-acetylglucosamine residues (68), and our results suggest that *O*-linked  $\beta$ -*N*-acetylglucosamylation may also occur in the bradyzoite/cyst stage.

The chitin-binding s-WGA lectin specifically recognizes *N*-acetylglucosamine-modified structures and does not bind to sialic acid residues like the WGA lectin (29). Previously, cysts were thought to possess chitin in the cyst wall based on evidence showing that (i) chitinase-treated cysts failed to bind s-WGA (24) and (ii) the cyst wall of chitinase-treated cysts was degraded, and bradyzoites were released (24, 30). These results demonstrated that s-WGA binding to the cyst wall is chitinase sensitive and support the hypothesis that the cyst wall-localized *N*-acetylglucosamine-modified molecule(s) recognized by s-WGA and chitinase is essential for the stability of the cyst wall and cysts. Thus, the molecules recognized by s-WGA and chitinase and the biological functions of these cyst wall-localized molecules are likely to be potential targets for cyst disruption and cyst elimination.

The only confirmed cyst wall molecule that is recognized and bound by s-WGA is an uncharacterized ~48-kDa cyst wall glycoprotein (23). Chitinases are glycosyl hydrolases that cleave the  $\beta$ -1,4 linkage of *N*-acetylglucosamine that is present in chitin and chitin-like oligosaccharide structures. The *Toxoplasma* cyst wall as well as the oocyst wall most likely do not contain chitin in view of the fact that *Toxoplasma* as well as its mammalian hosts do not express a chitin synthase (69, 70). Chitinase will not recognize *O*-linked *N*-acetylglucosamine residues since the requisite  $\beta$ -1,4 *N*-acetylglucosamine linkages required for chitinase activity are absent in *O*-linked glycoprotein modifications. Intriguingly, similar to the behavior of *Toxoplasma* cysts, chitinase treatment eliminated s-WGA/WGA binding of *Giardia* cysts (71). *Giardia* cysts also do not contain chitin, and the recognition of the *Giardia* cyst wall by s-WGA and WGA was previously attributed to the presence of short *N*-glycans in the cyst wall (70). *Toxoplasma* also has the capability of *N*-glycan modification of glycoproteins (72), although *N*-glycan modification in the cyst stage has not been previously investigated. It is plausible that the ~48-kDa *Toxoplasma* cyst wall glycoprotein that selectively binds s-WGA (23) is post-translationally modified by *N*-linked glycosylation that is recognized by s-WGA in a chitinase-sensitive manner. This hypothesis remains to be tested, as is whether the putative *N*-glycans that bind s-WGA and are recognized by chitinase are short *N*-glycans or bisected hybrid-type *N*-glycans with the chitobiose core of the oligosaccharide GlcNAc $\beta$ 1-4Man $\beta$ 1-4GlcNAc $\beta$ 1-4GlcNAc, which is known to be avidly bound by s-WGA and WGA (73, 74).

## MATERIALS AND METHODS

**Culture conditions and strains.** Type II Prugniaud (Pru)-background *Toxoplasma gondii* parasites were maintained *in vitro* by serial passage of tachyzoites in human foreskin fibroblast (HFF) monolayers (ATCC SCRS-1041.1) cultured in Eagle's modified essential medium (EMEM) (Lonza) containing 1% fetal bovine serum (FBS) (Life Technologies), 2 mM glutamine, 100 U/ml penicillin, and 100  $\mu$ g/ml streptomycin at 36°C in 95% air and 5% CO<sub>2</sub>. HFF cells were maintained in EMEM containing 10% FBS (HyClone), 2 mM glutamine, 100 U/ml penicillin, and 100  $\mu$ g/ml streptomycin at 37°C in 95% air and 5% CO<sub>2</sub>. The parental Pru strain Pru $\Delta$ ku80 was previously made transgenic for green fluorescent protein (GFP) under the control of the LDH2 bradyzoite-stage-specific promoter (75). The  $\Delta$ gra2 strain was previously developed using the Pru $\Delta$ ku80 knockout strain of the type II Pru strain (17, 76).

**In vitro cyst differentiation assay.** Tachyzoites were differentiated *in vitro* into bradyzoites within cysts essentially as previously and elegantly described by Tobin and colleagues (31). Differentiation medium contained RPMI medium without bicarbonate supplemented with 2.05 mM L-glutamine (HyClone), 20 mM HEPES-free acid (IBI Scientific), 1% XL-glutamine (a long-lasting stable form of glutamine; WWR), 1% FBS, and 1% penicillin-streptomycin. The pH of differentiation medium was adjusted to 8.1 with sodium hydroxide and the medium was filter sterilized. HFF cells were cultured on circular micro cover glass until confluent (Electron Microscopy Sciences), and confluent monolayers were infected with type II Pru parasites at a multiplicity of infection (MOI) of ~0.5. Infected HFF cells were washed once 3 h after infection in Dulbecco's phosphate-buffered saline (DPBS) supplemented with  $\text{Ca}^{2+}$  and  $\text{Mg}^{2+}$  and incubated in differentiation medium for 6 h, 1 day, 2 days, 3 days, 7 days, or 10 days at 37°C in ambient air. Medium was changed on day 3 and day 7.

**Cyst immunofluorescence assay and cyst location.** Infected cells were fixed in 4% paraformaldehyde for 10 min, and the excess was quenched with 0.1 M glycine. Infected cells were permeabilized and blocked in 3% FBS–0.2% Triton X-100 for 30 min, and this solution was used in all proceeding incubation steps. All samples were incubated with a 1:500 dilution of biotinylated, succinylated WGA (Vector Laboratories); a 1:25 dilution of primary mouse monoclonal anti-CST1 antibody (23); a 1:1,000 dilution of primary mouse monoclonal anti-GRA2 antibody (77); or a 1:1,000 dilution of primary rabbit anti-GRA4 (20) or anti-GRA6 (20) (antibodies were purchased from the Biotem Company, Apprieu, France, or kindly provided by L. D. Sibley, Washington University School of Medicine, St. Louis, MO, or L. M. Weiss, Albert Einstein College of Medicine, Bronx, NY). Preparations were washed three times with DPBS supplemented with  $\text{Ca}^{2+}$  and  $\text{Mg}^{2+}$  and incubated for 1 h at room temperature (RT) with a 1:1,000 dilution of secondary goat anti-rabbit IgG(H+L) (Thermo Fisher) and goat anti-mouse IgG(H+L) antibodies conjugated to Alexa Fluor 647 (Cell Signaling). All samples were incubated with a 1:200 dilution of DyLight 594 streptavidin (Vector Laboratories) for 1 h at RT. Samples were mounted in SlowFade gold antifade with 4',6-diamidino-2-phenylindole (DAPI) (Life Technologies) and then imaged with a Nikon A1R Si confocal microscope (Nikon, Inc.) using an Apo total internal-reflection fluorescence (TIRF) 100× oil differential interference contrast (DIC) N20 objective. Cysts were randomly selected for analysis by locating cysts using DIC microscopy. Bradyzoite differentiation in cysts was confirmed by GFP<sup>+</sup> bradyzoites. The focal plane (from a z-stack) selected for quantification was from the middle of the cyst, where the cyst size is maximal. Raw .nd2 files of cyst images were imported into Fiji for processing. Images were minimally processed for brightness (image → adjust → color balance) in Fiji (78). The colocalization of s-WGA with GRA4, GRA6, or CST1 was determined visually by analyzing each imaged cyst for spots of fluorescence overlap, and the percentage was calculated by the images that showed colocalization out of the total number of cysts imaged. The number of cysts for each strain analyzed in each experiment is reported in each figure legend.

**Cyst fluorescence intensity profiles.** Raw .nd2 image files were imported into Fiji to measure fluorescence intensity parallel to the cyst wall, as previously described (15). Images were cropped to isolate each cyst. A macro was written to generate a reliable mask of the cyst, slightly outside the cyst wall, using the s-WGA channel. The s-WGA channel was used to threshold the cyst, and holes were filled inside to obtain a continuous mask of the whole cyst. Successive layers were generated based on the original mask, growing or shrinking by dilate or erode morphological operations. Layers were generally 1 pixel thick. The fluorescence intensity of each region was measured for a selected fluorescence channel: s-WGA, CST1, GRA4, or GRA6. The macro generated layers within the cyst until the minimum area of the (shrinking) layer reached 1,000 square pixels. Layers were created by dilation to measure the fluorescence intensity outside the cyst, which provided the background fluorescence intensity. All data were imported into Excel to be further analyzed, as previously described (15). The calculated percent maximum fluorescence intensity and distance (micrometer) values were imported and graphed in Prism.

**Cyst wall definition and analysis.** The cyst wall region was identified and defined as previously described (15). The cyst wall outer region was identified by s-WGA, while the inner region was determined by GFP, which identifies the parasites within the cyst. The cyst wall region is defined by an outer and an inner boundary determined by the first point with <50% of the maximum fluorescence intensities of s-WGA and GFP, respectively. The cyst wall region is marked by dotted black lines, and the peak of s-WGA fluorescence is marked by a dotted red line. Next, we evaluated the location of CST1, GRA4, or GRA6 in comparison to the s-WGA-stained cyst wall using fluorescence intensities measured at the same time within the cyst. This cyst wall analysis was used to determine if two proteins were observed in the same layer.

**Cyst total fluorescence intensity quantification assay.** Raw .nd2 image files were imported into Fiji to measure the total fluorescence intensity at the cyst periphery and within the cyst interior, as previously described (15). The cyst periphery was determined to be the cyst wall plus two layers, which were added to include proteins near the cyst wall but not yet incorporated into the cyst wall. Fluorescence for s-WGA, CST1, GRA4, and GRA6 was measured in the  $\Delta ku80$  and  $\Delta gra2$  strains. To measure background fluorescence, a circle was drawn using the freehand selection tool, and fluorescence was measured outside the cyst on three different sides. All data were imported into Excel to be further analyzed, as previously described (15). All ratios were entered and graphed in Prism. A ratio of <1 means that there is a higher s-WGA, CST1, or GRA fluorescence intensity in the cyst interior than at the cyst periphery; a ratio of 1 represents s-WGA, CST1, or GRA fluorescence intensity at the cyst periphery equal to that in the cyst interior; and a ratio of >1 means that there is a higher s-WGA, CST1, or GRA fluorescence intensity at the cyst periphery than in the cyst interior. *P* values were calculated using Student's *t* test.

**Statistical analysis.** Unpaired *t* tests were used to calculate *P* values. All calculations of averages  $\pm$  standard errors of the means (SEM) and *P* values were performed using GraphPad Prism software version 5.0c.

## SUPPLEMENTAL MATERIAL

Supplemental material is available online only.

**FIG S1**, TIF file, 1.7 MB.

**FIG S2**, TIF file, 1.9 MB.

**FIG S3**, TIF file, 1.3 MB.

## ACKNOWLEDGMENTS

We are grateful to Zdenek Svindrych for writing the Fiji macro used for quantification of cyst images acquired using confocal microscopy and the BioMT Core imaging facility for training and advice. We thank L. D. Sibley (Washington University School of Medicine, St. Louis, MO) and L. M. Weiss (Albert Einstein College of Medicine, Bronx, NY) for sharing antibodies used in this study.

This work was supported by National Institutes of Health (NIH) grants AI105563, AI108489, AI131630, and AI137118 to D.J.B. R.B.G. was a trainee on NIH grants T32AI007519 and T32AI007363. The BioMT Core (imaging core facility) was supported by the National Institute of General Medical Sciences (NIGMS) (P20GM113132).

R.B.G., B.A.F., and D.J.B. conceptualized the experiments. R.B.G. performed the experiments and analyzed the data. All authors contributed to writing, reviewing, and editing the manuscript.

## REFERENCES

- Flegr J, Prandota J, Sovickova M, Israili ZH. 2014. Toxoplasmosis—a global threat. Correlation of latent toxoplasmosis with specific disease burden in a set of 88 countries. *PLoS One* 9:e90203. <https://doi.org/10.1371/journal.pone.0090203>.
- Ferguson DJ. 2004. Use of molecular and ultrastructural markers to evaluate stage conversion of *Toxoplasma gondii* in both the intermediate and definitive host. *Int J Parasitol* 34:347–360. <https://doi.org/10.1016/j.ijpara.2003.11.024>.
- Tenter AM, Heckeroth AR, Weiss LM. 2000. *Toxoplasma gondii*: from animals to humans. *Int J Parasitol* 30:1217–1258. [https://doi.org/10.1016/S0020-7519\(00\)00124-7](https://doi.org/10.1016/S0020-7519(00)00124-7).
- Lass A, Ma L, Kontogeorgos I, Zhang X, Li X, Karanis P. 2019. First molecular detection of *Toxoplasma gondii* in vegetable samples in China using qualitative, quantitative real-time PCR and multilocus genotyping. *Sci Rep* 9:17581. <https://doi.org/10.1038/s41598-019-54073-6>.
- Khan K, Khan W. 2018. Congenital toxoplasmosis: an overview of the neurological and ocular manifestations. *Parasitol Int* 67:715–721. <https://doi.org/10.1016/j.parint.2018.07.004>.
- Hutson SL, Wheeler KM, McLone D, Frim D, Penn R, Swisher CN, Heydemann PT, Boyer KM, Noble AG, Rabiah P, Withers S, Montoya JG, Wroblewski K, Karrison T, Grigg ME, McLeod R. 2015. Patterns of hydrocephalus caused by congenital *Toxoplasma gondii* infection associate with parasite genetics. *Clin Infect Dis* 61:1831–1834. <https://doi.org/10.1093/cid/civ720>.
- McLeod R, Boyer KM, Lee D, Mui E, Wroblewski K, Karrison T, Noble AG, Withers S, Swisher CN, Heydemann PT, Sautter M, Babiarz J, Rabiah P, Meier P, Grigg ME, Toxoplasmosis Study Group. 2012. Prematurity and severity are associated with *Toxoplasma gondii* alleles (NCCCTS, 1981–2009). *Clin Infect Dis* 54:1595–1605. <https://doi.org/10.1093/cid/cis258>.
- Luft BJ, Remington JS. 1992. Toxoplasmic encephalitis in AIDS. *Clin Infect Dis* 15:211–222. <https://doi.org/10.1093/clinids/15.2.211>.
- Weiss LM, Dubey JP. 2009. Toxoplasmosis: a history of clinical observations. *Int J Parasitol* 39:895–901. <https://doi.org/10.1016/j.ijpara.2009.02.004>.
- Kafsack BF, Pena JD, Coppens I, Ravindran S, Boothroyd JC, Carruthers VB. 2009. Rapid membrane disruption by a perforin-like protein facilitates parasite exit from host cells. *Science* 323:530–533. <https://doi.org/10.1126/science.1165740>.
- Caldas LA, Attias M, de Souza W. 2018. A structural analysis of the natural egress of *Toxoplasma gondii*. *Microbes Infect* 20:57–62. <https://doi.org/10.1016/j.micinf.2017.09.006>.
- Guevara RB, Fox BA, Bzik DJ. 2020. *Toxoplasma gondii* parasitophorous vacuole membrane-associated dense granule proteins regulate maturation of the cyst wall. *mSphere* 5:e00851-19. <https://doi.org/10.1128/mSphere.00851-19>.
- Lemgruber L, Lupetti P, Martins-Duarte ES, De Souza W, Vommaro RC. 2011. The organization of the wall filaments and characterization of the matrix structures of *Toxoplasma gondii* cyst form. *Cell Microbiol* 13:1920–1932. <https://doi.org/10.1111/j.1462-5822.2011.01681.x>.
- Ferguson DJ, Hutchison WM. 1987. An ultrastructural study of the early development and tissue cyst formation of *Toxoplasma gondii* in the brains of mice. *Parasitol Res* 73:483–491. <https://doi.org/10.1007/bf00535321>.
- Guevara RB, Fox BA, Falla A, Bzik DJ. 2019. *Toxoplasma gondii* intravacuolar-network-associated dense granule proteins regulate maturation of the cyst matrix and cyst wall. *mSphere* 4:e00487-19. <https://doi.org/10.1128/mSphere.00487-19>.
- Tu V, Mayoral J, Sugi T, Tomita T, Han B, Ma YF, Weiss LM. 2019. Enrichment and proteomic characterization of the cyst wall from in vitro *Toxoplasma gondii* cysts. *mBio* 10:e00469-19. <https://doi.org/10.1128/mBio.00469-19>.
- Guevara RB, Rommereim LM, Falla A, Bellini V, Petre G, Rak C, Cantillana V, Dubremetz JF, Cesbron-Delauw MF, Taylor GA, Mercier C, Bzik DJ. 2019. *Toxoplasma gondii* parasitophorous vacuole membrane-associated dense granule proteins orchestrate chronic infection and GRA12 underpins resistance to host gamma interferon. *mBio* 10:e00589-19. <https://doi.org/10.1128/mBio.00589-19>.
- Fox BA, Falla A, Rommereim LM, Tomita T, Gigley JP, Mercier C, Cesbron-Delauw MF, Weiss LM, Bzik DJ. 2011. Type II *Toxoplasma gondii* KU80 knockout strains enable functional analysis of genes required for cyst development and latent infection. *Eukaryot Cell* 10:1193–1206. <https://doi.org/10.1128/EC.00297-10>.
- Tomita T, Bzik DJ, Ma YF, Fox BA, Markillie LM, Taylor RC, Kim K, Weiss LM. 2013. The *Toxoplasma gondii* cyst wall protein CST1 is critical for cyst wall integrity and promotes bradyzoite persistence. *PLoS Pathog* 9:e1003823. <https://doi.org/10.1371/journal.ppat.1003823>.
- Labruyere E, Lingnau M, Mercier C, Sibley LD. 1999. Differential membrane targeting of the secretory proteins GRA4 and GRA6 within the parasitophorous vacuole formed by *Toxoplasma gondii*. *Mol Biochem Parasitol* 102:311–324. [https://doi.org/10.1016/S0166-6851\(99\)00092-4](https://doi.org/10.1016/S0166-6851(99)00092-4).
- Mercier C, Dubremetz JF, Rauscher B, Lecordier L, Sibley LD, Cesbron-Delauw MF. 2002. Biogenesis of nanotubular network in *Toxoplasma*

- parasitophorous vacuole induced by parasite proteins. *Mol Biol Cell* 13:2397–2409. <https://doi.org/10.1091/mbc.e02-01-0021>.
22. Sethi KK, Rahman A, Pelster B, Brandis H. 1997. Search for the presence of lectin-binding sites on *Toxoplasma gondii*. *J Parasitol* 63:1076–1080. <https://doi.org/10.2307/3279850>.
  23. Zhang YW, Halonen SK, Ma YF, Wittner M, Weiss LM. 2001. Initial characterization of CST1, a *Toxoplasma gondii* cyst wall glycoprotein. *Infect Immun* 69:501–507. <https://doi.org/10.1128/IAI.69.1.501-507.2001>.
  24. Boothroyd JC, Black M, Bonnefoy S, Hehl A, Knoll LJ, Manger ID, Ortega-Barria E, Tomavo S. 1997. Genetic and biochemical analysis of development in *Toxoplasma gondii*. *Philos Trans R Soc Lond B Biol Sci* 352:1347–1354. <https://doi.org/10.1098/rstb.1997.0119>.
  25. Hammarstrom S, Murphy LA, Goldstein IJ, Etzler ME. 1977. Carbohydrate binding specificity of four N-acetyl-D-galactosamine-“specific” lectins: Helix pomatia A hemagglutinin, soy bean agglutinin, lima bean lectin, and Dolichos biflorus lectin. *Biochemistry* 16:2750–2755. <https://doi.org/10.1021/bi00631a025>.
  26. Tomita T, Sugi T, Yakubu R, Tu V, Ma Y, Weiss LM. 2017. Making home sweet and sturdy: *Toxoplasma gondii* ppGalNac-Ts glycosylate in hierarchical order and confer cyst wall rigidity. *mBio* 8:e02048-16. <https://doi.org/10.1128/mBio.02048-16>.
  27. Caffaro CE, Koshy AA, Liu L, Zeiner GM, Hirschberg CB, Boothroyd JC. 2013. A nucleotide sugar transporter involved in glycosylation of the *Toxoplasma* tissue cyst wall is required for efficient persistence of bradyzoites. *PLoS Pathog* 9:e1003331. <https://doi.org/10.1371/journal.ppat.1003331>.
  28. Tomita T, Ma Y, Weiss L. 2018. Characterization of a SRS13: a new cyst wall mucin-like domain containing protein. *Parasitol Res* 117:2457–2466. <https://doi.org/10.1007/s00436-018-5934-3>.
  29. Monsigny M, Roche AC, Sene C, Maget-Dana R, Delmotte F. 1980. Sugar-lectin interactions: how does wheat-germ agglutinin bind sialoglycoconjugates? *Eur J Biochem* 104:147–153. <https://doi.org/10.1111/j.1432-1033.1980.tb04410.x>.
  30. Nance JP, Vannella KM, Worth D, David C, Carter D, Noor S, Hubeau C, Fitz L, Lane TE, Wynn TA, Wilson EH. 2012. Chitinase dependent control of protozoan cyst burden in the brain. *PLoS Pathog* 8:e1002990. <https://doi.org/10.1371/journal.ppat.1002990>.
  31. Tobin C, Pollard A, Knoll L. 2010. *Toxoplasma gondii* cyst wall formation in activated bone marrow-derived macrophages and bradyzoite conditions. *J Vis Exp* 2010:2091. <https://doi.org/10.3791/2091>.
  32. Weiss LM, Kim K. 2000. The development and biology of bradyzoites of *Toxoplasma gondii*. *Front Biosci* 5:D391–D405. <https://doi.org/10.2741/A521>.
  33. Fux B, Nawas J, Khan A, Gill DB, Su C, Sibley LD. 2007. *Toxoplasma gondii* strains defective in oral transmission are also defective in developmental stage differentiation. *Infect Immun* 75:2580–2590. <https://doi.org/10.1128/IAI.00085-07>.
  34. Sahm M, Fischer HG, Gross U, Reiter-Owona I, Seitz HM. 1997. Cyst formation by *Toxoplasma gondii* in vivo and in brain-cell culture: a comparative morphology and immunocytochemistry study. *Parasitol Res* 83:659–665. <https://doi.org/10.1007/s004360050315>.
  35. Jelenska J, Crawford MJ, Harb OS, Zuther E, Haselkorn R, Roos DS, Gornicki P. 2001. Subcellular localization of acetyl-CoA carboxylase in the apicomplexan parasite *Toxoplasma gondii*. *Proc Natl Acad Sci U S A* 98:2723–2728. <https://doi.org/10.1073/pnas.051629998>.
  36. Chen AL, Kim EW, Toh JY, Vashisht AA, Rashoff AQ, Van C, Huang AS, Moon AS, Bell HN, Bentolila LA, Wohlschlegel JA, Bradley PJ. 2015. Novel components of the *Toxoplasma* inner membrane complex revealed by BioID. *mBio* 6:e02357-14. <https://doi.org/10.1128/mBio.02357-14>.
  37. Seidi A, Muellner-Wong LS, Rajendran E, Tjhin ET, Dagley LF, Aw YY, Faou P, Webb AI, Tonkin CJ, van Dooren GG. 2018. Elucidating the mitochondrial proteome of *Toxoplasma gondii* reveals the presence of a divergent cytochrome c oxidase. *Elife* 7:e38131. <https://doi.org/10.7554/eLife.38131>.
  38. Coppin A, Dzierzinski F, Legrand S, Mortuaire M, Ferguson D, Tomavo S. 2003. Developmentally regulated biosynthesis of carbohydrate and storage polysaccharide during differentiation and tissue cyst formation in *Toxoplasma gondii*. *Biochimie* 85:353–361. [https://doi.org/10.1016/s0300-9084\(03\)00076-2](https://doi.org/10.1016/s0300-9084(03)00076-2).
  39. Lujan HD, Mowatt MR, Nash TE. 1997. Mechanisms of *Giardia lamblia* differentiation into cysts. *Microbiol Mol Biol Rev* 61:294–304. <https://doi.org/10.1128/61.3.294-304.1997>.
  40. Cabral CM, Tuladhar S, Dietrich HK, Nguyen E, MacDonald WR, Trivedi T, Devineni A, Koshy AA. 2016. Neurons are the primary target cell for the brain-tropic intracellular parasite *Toxoplasma gondii*. *PLoS Pathog* 12:e1005447. <https://doi.org/10.1371/journal.ppat.1005447>.
  41. Koshy AA, Cabral CM. 2014. 3-D imaging and analysis of neurons infected in vivo with *Toxoplasma gondii*. *J Vis Exp* 2014:52237. <https://doi.org/10.3791/52237>.
  42. Fox BA, Gigley JP, Bzik DJ. 2004. *Toxoplasma gondii* lacks the enzymes required for de novo arginine biosynthesis and arginine starvation triggers cyst formation. *Int J Parasitol* 34:323–331. <https://doi.org/10.1016/j.ijpara.2003.12.001>.
  43. Bohne W, Heesemann J, Gross U. 1994. Reduced replication of *Toxoplasma gondii* is necessary for induction of bradyzoite-specific antigens: a possible role for nitric oxide in triggering stage conversion. *Infect Immun* 62:1761–1767. <https://doi.org/10.1128/IAI.62.5.1761-1767.1994>.
  44. Augusto L, Martynowicz J, Staschke KA, Wek RC, Sullivan WJ, Jr. 2018. Effects of PERK eIF2alpha kinase inhibitor against *Toxoplasma gondii*. *Antimicrob Agents Chemother* 62:e01442-18. <https://doi.org/10.1128/AAC.01442-18>.
  45. Radke JB, Worth D, Hong D, Huang S, Sullivan WJ, Jr, Wilson EH, White MW. 2018. Transcriptional repression by ApiAP2 factors is central to chronic toxoplasmosis. *PLoS Pathog* 14:e1007035. <https://doi.org/10.1371/journal.ppat.1007035>.
  46. Huang S, Holmes MJ, Radke JB, Hong DP, Liu TK, White MW, Sullivan WJ, Jr. 2017. *Toxoplasma gondii* AP2IX-4 regulates gene expression during bradyzoite development. *mSphere* 2:e00054-17. <https://doi.org/10.1128/mSphere.00054-17>.
  47. Frenkel JK. 1956. Pathogenesis of toxoplasmosis and of infections with organisms resembling *Toxoplasma*. *Ann N Y Acad Sci* 64:215–251. <https://doi.org/10.1111/j.1749-6632.1956.tb36616.x>.
  48. Sugi T, Tu V, Ma Y, Tomita T, Weiss LM. 2017. *Toxoplasma gondii* requires glycogen phosphorylase for balancing amylopectin storage and for efficient production of brain cysts. *mBio* 8:e01289-17. <https://doi.org/10.1128/mBio.01289-17>.
  49. Uboldi AD, McCoy JM, Blume M, Gerlic M, Ferguson DJ, Dagley LF, Beahan CT, Stapleton DI, Gooley PR, Bacic A, Masters SL, Webb AI, McConville MJ, Tonkin CJ. 2015. Regulation of starch stores by a Ca(2+)-dependent protein kinase is essential for viable cyst development in *Toxoplasma gondii*. *Cell Host Microbe* 18:670–681. <https://doi.org/10.1016/j.chom.2015.11.004>.
  50. Radke JB, Lucas O, De Silva EK, Ma Y, Sullivan WJ, Jr, Weiss LM, Llinas M, White MW. 2013. ApiAP2 transcription factor restricts development of the *Toxoplasma* tissue cyst. *Proc Natl Acad Sci U S A* 110:6871–6876. <https://doi.org/10.1073/pnas.1300059110>.
  51. Buchholz KR, Fritz HM, Chen X, Durbin-Johnson B, Rocke DM, Ferguson DJ, Conrad PA, Boothroyd JC. 2011. Identification of tissue cyst wall components by transcriptome analysis of in vivo and in vitro *Toxoplasma gondii* bradyzoites. *Eukaryot Cell* 10:1637–1647. <https://doi.org/10.1128/EC.05182-11>.
  52. Watts E, Zhao Y, Dhara A, Eller B, Patwardhan A, Sinai AP. 2015. Novel approaches reveal that *Toxoplasma gondii* bradyzoites within tissue cysts are dynamic and replicating entities in vivo. *mBio* 6:e01155-15. <https://doi.org/10.1128/mBio.01155-15>.
  53. Tu V, Yakubu R, Weiss LM. 2018. Observations on bradyzoite biology. *Microbes Infect* 20:466–476. <https://doi.org/10.1016/j.micinf.2017.12.003>.
  54. Herrera-Martinez M, Hernandez-Ramirez VI, Lagunes-Guillen AE, Chavez-Munguia B, Talamas-Rohana P. 2013. Actin, RhoA, and Rab11 participation during encystment in *Entamoeba* invaders. *Biomed Res Int* 2013:919345. <https://doi.org/10.1155/2013/919345>.
  55. Castillo-Romero A, Leon-Avila G, Wang CC, Perez Rangel A, Camacho Nuez M, Garcia Tovar C, Ayala-Sumano JT, Luna-Arias JP, Hernandez JM. 2010. Rab11 and actin cytoskeleton participate in *Giardia lamblia* encystation, guiding the specific vesicles to the cyst wall. *PLoS Negl Trop Dis* 4:e697. <https://doi.org/10.1371/journal.pntd.0000697>.
  56. Krtkova J, Thomas EB, Alas GC, Schraner EM, Behjatnia HR, Hehl AB, Paredes AR. 2016. Rac regulates *Giardia lamblia* encystation by coordinating cyst wall protein trafficking and secretion. *mBio* 7:e01003-16. <https://doi.org/10.1128/mBio.01003-16>.
  57. Shukla A, Olszewski KL, Llinas M, Rommereim LM, Fox BA, Bzik DJ, Xia D, Wastling J, Beiting D, Roos DS, Shanmugam D. 2018. Glycolysis is important for optimal asexual growth and formation of mature tissue cysts by *Toxoplasma gondii*. *Int J Parasitol* 48:955–968. <https://doi.org/10.1016/j.ijpara.2018.05.013>.
  58. Rommereim LM, Bellini V, Fox BA, Petre G, Rak C, Touquet B, Aldebert D, Dubremetz JF, Cesbron-Delauw MF, Mercier C, Bzik DJ. 2016. Phenotypes

- associated with knockouts of eight dense granule gene loci (GRA2-9) in virulent *Toxoplasma gondii*. *PLoS One* 11:e0159306. <https://doi.org/10.1371/journal.pone.0159306>.
59. Lopez J, Bittame A, Massera C, Vasseur V, Effantin G, Valat A, Buailon C, Allart S, Fox BA, Rommereim LM, Bzik DJ, Schoehn G, Weissenhorn W, Dubremetz JF, Gagnon J, Mercier C, Cesbron-Delauw MF, Blanchard N. 2015. Intravacuolar membranes regulate CD8 T cell recognition of membrane-bound *Toxoplasma gondii* protective antigen. *Cell Rep* 13: 2273–2286. <https://doi.org/10.1016/j.celrep.2015.11.001>.
  60. Gas-Pascual E, Ichikawa HT, Sheikh MO, Serji MI, Deng B, Mandalasi M, Bandini G, Samuelson J, Wells L, West CM. 2019. CRISPR/Cas9 and glycomics tools for *Toxoplasma* glycobiochemistry. *J Biol Chem* 294: 1104–1125. <https://doi.org/10.1074/jbc.RA118.006072>.
  61. West CM, Blader IJ. 2015. Oxygen sensing by protozoans: how they catch their breath. *Curr Opin Microbiol* 26:41–47. <https://doi.org/10.1016/j.mib.2015.04.006>.
  62. Rahman K, Zhao P, Mandalasi M, van der Wel H, Wells L, Blader IJ, West CM. 2016. The E3 ubiquitin ligase adaptor protein Skp1 is glycosylated by an evolutionarily conserved pathway that regulates protist growth and development. *J Biol Chem* 291:4268–4280. <https://doi.org/10.1074/jbc.M115.703751>.
  63. Gajria B, Bahl A, Brestelli J, Dommer J, Fischer S, Gao X, Heiges M, Iodice J, Kissinger JC, Mackey AJ, Pinney DF, Roos DS, Stoeckert CJ, Jr, Wang H, Brunk BP. 2008. ToxoDB: an integrated *Toxoplasma gondii* database resource. *Nucleic Acids Res* 36:D553–D556. <https://doi.org/10.1093/nar/gkm981>.
  64. Bandini G, Albuquerque-Wendt A, Hegermann J, Samuelson J, Routier FH. 2019. Protein O- and C-glycosylation pathways in *Toxoplasma gondii* and *Plasmodium falciparum*. *Parasitology* 146:1755–1766. <https://doi.org/10.1017/S0031182019000040>.
  65. Perez-Cervera Y, Harichaux G, Schmidt J, Debierre-Grockiego F, Dehennaut V, Bieker U, Meurice E, Lefebvre T, Schwarz RT. 2011. Direct evidence of O-GlcNAcylation in the apicomplexan *Toxoplasma gondii*: a biochemical and bioinformatic study. *Amino Acids* 40:847–856. <https://doi.org/10.1007/s00726-010-0702-4>.
  66. Lefebvre T, Issad T. 2015. 30 years old: O-GlcNAc reaches the age of reason—regulation of cell signaling and metabolism by O-GlcNAcylation. *Front Endocrinol (Lausanne)* 6:17. <https://doi.org/10.3389/fendo.2015.00017>.
  67. Lefebvre T, Dehennaut V, Guinez C, Olivier S, Drougat L, Mir AM, Mortuaire M, Vercoutter-Edouart AS, Michalski JC. 2010. Dysregulation of the nutrient/stress sensor O-GlcNAcylation is involved in the etiology of cardiovascular disorders, type-2 diabetes and Alzheimer's disease. *Biochim Biophys Acta* 1800:67–79. <https://doi.org/10.1016/j.bbagen.2009.08.008>.
  68. Aquino-Gil MO, Kupferschmid M, Shams-Eldin H, Schmidt J, Yamakawa N, Mortuaire M, Krzewinski F, Hardville S, Zenteno E, Rolando C, Bray F, Perez Campos E, Dubremetz JF, Perez-Cervera Y, Schwarz RT, Lefebvre T. 2018. Apart from rhoptries, identification of *Toxoplasma gondii*'s O-GlcNAcylated proteins reinforces the universality of the O-GlcNAcome. *Front Endocrinol (Lausanne)* 9:450. <https://doi.org/10.3389/fendo.2018.00450>.
  69. Bushkin GG, Motari E, Carpentieri A, Dubey JP, Costello CE, Robbins PW, Samuelson J. 2013. Evidence for a structural role for acid-fast lipids in oocyst walls of *Cryptosporidium*, *Toxoplasma*, and *Eimeria*. *mBio* 4:e00387-13. <https://doi.org/10.1128/mBio.00387-13>.
  70. Samuelson J, Bushkin GG, Chatterjee A, Robbins PW. 2013. Strategies to discover the structural components of cyst and oocyst walls. *Eukaryot Cell* 12:1578–1587. <https://doi.org/10.1128/EC.00213-13>.
  71. Ward HD, Alroy J, Lev BI, Keusch GT, Pereira ME. 1985. Identification of chitin as a structural component of *Giardia* cysts. *Infect Immun* 49: 629–634. <https://doi.org/10.1128/IAI.49.3.629-634.1985>.
  72. Bushkin GG, Ratner DM, Cui J, Banerjee S, Duraisingh MT, Jennings CV, Dvorin JD, Gubbels M-J, Robertson SD, Steffen M, O'Keefe BR, Robbins PW, Samuelson J. 2010. Suggestive evidence for Darwinian selection against asparagine-linked glycans of *Plasmodium falciparum* and *Toxoplasma gondii*. *Eukaryot Cell* 9:228–241. <https://doi.org/10.1128/EC.00197-09>.
  73. Itakura Y, Nakamura-Tsuruta S, Kominami J, Tateno H, Hirabayashi J. 2017. Sugar-binding profiles of chitin-binding lectins from the Hevein family: a comprehensive study. *Int J Mol Sci* 18:1160. <https://doi.org/10.3390/ijms18061160>.
  74. Yamamoto K, Tsuji T, Matsumoto I, Osawa T. 1981. Structural requirements for the binding of oligosaccharides and glycopeptides to immobilized wheat germ agglutinin. *Biochemistry* 20:5894–5899. <https://doi.org/10.1021/bi00523a037>.
  75. Singh U, Brewer JL, Boothroyd JC. 2002. Genetic analysis of tachyzoite to bradyzoite differentiation mutants in *Toxoplasma gondii* reveals a hierarchy of gene induction. *Mol Microbiol* 44:721–733. <https://doi.org/10.1046/j.1365-2958.2002.02903.x>.
  76. Fox BA, Ristuccia JG, Gigley JP, Bzik DJ. 2009. Efficient gene replacements in *Toxoplasma gondii* strains deficient for nonhomologous end joining. *Eukaryot Cell* 8:520–529. <https://doi.org/10.1128/EC.00357-08>.
  77. Torpier G, Charif H, Darcy F, Liu J, Darde ML, Capron A. 1993. *Toxoplasma gondii*: differential location of antigens secreted from encysted bradyzoites. *Exp Parasitol* 77:13–22. <https://doi.org/10.1006/expr.1993.1056>.
  78. Schindelin J, Arganda-Carreras I, Frise E, Kaynig V, Longair M, Pietzsch T, Preibisch S, Rueden C, Saalfeld S, Schmid B, Tinevez JY, White DJ, Hartenstein V, Eliceiri K, Tomancak P, Cardona A. 2012. Fiji: an open-source platform for biological-image analysis. *Nat Methods* 9:676–682. <https://doi.org/10.1038/nmeth.2019>.